scientific reports

Check for updates

OPEN

Electrospun polycaprolactone nanofibrous membranes loaded with baicalin for antibacterial wound dressing

Weiwei Zeng[1,2,6], Nga-man Cheng[3,6], Xia Liang[2], Haofeng Hu[4], Fulin Luo[4], Jia Jin[4]✉ & Ya-wei Li[5]✉

Due to the rise in bacterial resistance, the antibacterial extractions from Chinese herbs have been used more frequently for wound care. In this work, baicalin, an extraction from the Chinese herb *Scutellaria baicalensis*, was utilized as the antibacterial component in the poly(ε-caprolactone)/MXene (PCL/$Ti_3C_2T_X$) hybrid nanofibrous membranes for wound dressing. The results revealed that the presence of $Ti_3C_2T_X$ aided in the diameter reduction of the electrospun nanofibers. The PCL hybrid membrane containing 3 wt% $Ti_3C_2T_X$ nanoflakes and 5 wt% baicalin exhibited the smallest mean diameter of 210 nm. Meanwhile, the antibacterial tests demonstrated that the PCL ternary hybrid nanofibers containing $Ti_3C_2T_X$ and baicalin exhibited adequate antibacterial activity against the Gram-positive bacterial *S. aureus* due to the good synergistic effects of $Ti_3C_2T_X$ naoflakes and baicalin. The addition of $Ti_3C_2T_X$ nanoflakes and baicalin could significantly improve the hydrophilicity of the membranes, resulting in the release of baicalin from the nanofibers. In addition, the cytotoxicity of the nanofibers on rat skeletal myoblast L6 cells confirmed their good compatibility with these PCL-based nanofibrous membrances. This work offers a feasible way to prepare antibacterial nanofibrous membranes using Chinese herb extraction for wound dressing applications.

The skin is the first barrier for the human body to protect the internal organs against microorganisms or other external hazards[1]. However, the skin is highly susceptible to damage due to injury or illness. Cutaneous wounds are easily infected, resulting in a massive burden on the healthcare system[2]. Traditional wound dressing materials such as cellulose, silk, alginate, collagen, and so forth, have no ability to inhibit bacteria colonization or avoid microorganisms' growth[3–5]. Therefore, there is a need for antibacterial wound dressings to prevent cutaneous wound contamination. Recently, electrospun nanofiber scaffolds have attracted considerable attention in the field of wound dressings due to their unique characteristics, such as high oxygen permittivity, high tensile strength, diverse morphological features, tunable porosity and tailored ability[6]. Antibacterial ingredients such as antibiotics, metal oxides, and active carbon nanoparticles are being incorporated into the fibrous matrix to aid in the healing of cutaneous wounds[7,8].

Poly(ε-caprolactone) (PCL) is a type of biodegradable and biocompatible aliphatic linear polyester that can be synthesized by the ring-opening polymerization of ε-caprolactone. PCL has received considerable attention due to its high toughness, biodegradability, and biocompatibility. It has been demonstrated that electrospun PCL nanofibrous scaffolds can be utilized for wound dressing applications[9–11]. The native porous structure characteristics of PCL scaffolds can mimic the skin's extracellular matrix (ECM) structural properties while also providing high oxygen permeability. In order to confer antibacterial capabilities on the PCL nanofibrous scaffolds, different types of metal oxides or metals have been introduced into the PCL matrices[12]. Zhu et al. found that the insertion of silver (Ag) and magnesium (Mg) ions into gelatin/polycaprolactone (GT/PCL) could endow the nanofibers with antibacterial activity as well as pro-angiogenesis function, which benefited for skin wound repair[13]. Ghiyasi and his colleagues discovered that the hybrid scaffolds consisting of Urtica dioica, ZnO nanoparticles and PCL

[1]The Second People's Hospital of Longgang District, Shenzhen 518112, China. [2]Shenzhen Baoan Women's and Children's Hospital, Jinan University, Shenzhen 518102, China. [3]Accident and Emergency Medicine Academic Unit, The Chinese University of Hong Kong, Hong Kong, SAR, China. [4]College of Life Sciences and Medicine, Zhejiang Sci-Tech University, Hangzhou 310018, China. [5]Lianshui People's Hospital, Affiliated to Kangda College of Nanjing Medical University, Huaian 223400, China. [6]These authors contributed equally: Weiwei Zeng and Nga-man Cheng. ✉email: aukaukauk@163.com; lyw_20120220@163.com

had good antibacterial activity against *E. coli* and *S. aureus*[14]. In addition, the nanofiber of the hybrid scaffold exhibited good biocompatibility and cell adhesion to fibroblast L929 cells in vivo tests. Ekram et al. demonstrated that the presence of zinc chloride ($ZnCl_2$) reduced the diameter of the PCL/$ZnCl_2$ nanofibers while increasing the degradation rate and mechanical properties[15]. Moreover, the antibacterial composite nanofiber was found to greatly boost the proliferation of stem cells. Trcin et al. found that the PCL scaffolds containing TiO_2 nanoparticles could provide statistically significant antimicrobial activity against different types of bacteria[16]. Furthermore, the PCL/TiO_2 scaffolds with a maximum porosity of 93%, on the other hand, were found to be capable of supporting the adhesion and proliferation of limbal stem cells.

MXene is a new family of two-dimensional (2D) materials that integrates the transition metals M (Ti, Cr, V, Nb and Mo etc.) with huge amounts of X (carbides, nitrides, or carbonitrides) by removing the A-element in the MAX phase[17,18]. MXene ($Ti_3C_2T_X$) exhibits superior biocompatibility and antibacterial efficiency against both Gram-negative and Gram-positive bacteria than graphene oxide due to its ultrathin structure and unique physiochemical properties[19,20]. Awasthi et al. found that the addition of MXene into PCL nanofibers maintained good biocompatibility in vitro with ibroblasts (NIH-3T3) and preosteoblasts (MC3T3-E1) cell lines[21]. In addition, the presence of $Ti_3C_2T_X$ nanosheets contributed to reducing the diameter and improving the morphology of PCL/$Ti_3C_2T_X$ nanofibers. However, no data on the antibacterial activities of PCL/$Ti_3C_2T_X$ nanofibers have been reported to far.

Herbal extracts have been widely utilized to cure various diseases since ancient times. Plant-derived phytochemicals can serve as potential antibacides with fewer side effects. Baicalin, a flavonoid extracted from the Chinese herb Scutellaria baicalensis, has been regarded as a multitherapeutic agent in the field of biomedicine[22]. It shows various positive benefits on wounds, including anti-oxidative, anti-bacterial, and anti-inflammatory properties[23,24]. However, little research has been performed to date on the use of baicalin in electrospun fibers for wound dressings.

In this work, MXene ($Ti_3C_2T_X$) was first exfoliated to obtain $Ti_3C_2T_X$ nanoflakes. Then the resulting $Ti_3C_2T_X$ nanoflakes were incorporated into the PCL matrix with herbal extraction baicalin by electrospinning. The morphology, thermal stability, hydrophilicity, and mechanical properties of the electrospun nanofibers consisting of PCL/$Ti_3C_2T_X$/baicalin ternary composites were investigated. The addition of $Ti_3C_2T_X$ and baicalin was expected to have synergistic effects on improving the wound dressing's antibacterial performance against gram-positive bacterial *S. aureus*. Furthermore, the biocompatibility in vitro of this wound dressing was also evaluated by using rat skeletal myoblast L6 cells.

Materials and methods

Materials. Poly(ε-caprolactone) (PCL, CapaTM 6800) with a mean molecular weight of 80,000 was obtained from Weibo Chemical Co., Ltd. (Guangzhou, China). MXene ($Ti_3C_2T_X$) with 400 meshes was supplied by Beike 2D materials Co., Ltd. (Beijing, China). Baicalin (purity > 95%) was supplied by Macklin Biochemical Co., Ltd. (Shanghai, China). Chloroform and dimethylformamide (DMF) were purchased from J&K (Beijing, China).

Preparation of electrospun PCL composite nanofibrous membranes. The exfoliation of $Ti_3C_2T_X$ was performed by high energy ball milling using a Miqi YXQM-1L planetary micromill (Changsha, China). $Ti_3C_2T_X$ (4 g) and zirconium oxide milling balls (70 g) were placed in a 250 ml grinding bowl and performed at 600 rpm for 4 h. Then the exfoliated $Ti_3C_2T_X$ was removed from the grinding bowl with DI water, followed by sonication in DI water for 30 min to exfoliate completely. Finally, the resulting $Ti_3C_2T_X$ nanoflakes were centrifuged at 3500 rpm for 10 min, and the obtained suspension was freeze-dried overnight.

The electrospun nanofibers of the PCL/$Ti_3C_2T_X$/baicalin ternary composite were prepared using a commercially available electrospinning machine (TL-Pro, Tongli Weina Co., Ltd., Shenzhen, China), as shown in Fig. 1. The formulations of PCL based nanofibers are shown in Table 1. The concentration of PCL was fixed at 100 mg/mL in a mixed chloroform/DMF (8:2, v/v) solution. Subsequently, the desired amount of $Ti_3C_2T_X$ and baicalin was added into the PCL solution with vigorous stirring. The prepared PCL solution was loaded into a 10 mL plastic syringe with a metal capillary needle (0.50 mm inner diameter, and 30 mm length). The applied electrospinning voltage was fixed at 15 kV and the flow rate was kept at 1 mL/h. The obtained nanofibers were subsequently placed in a vacuum oven at 50 ℃ for 6 h to remove the remaining solvent.

Scanning electron microscope (SEM) observation. The morphology of $Ti_3C_2T_X$ and the prepared nanofibers was observed by a scanning electron microscope (SEM, FEI Quata 250, USA). Prior to observation, the specimens were sputtered with a thin layer of gold to avoid charge accumulation.

Atomic force microscope (AFM) observation. The thickness of $Ti_3C_2T_X$ nanoflakes was measured by an atomic force microscopy (AFM, VEECO Multimode V, USA) with tapping mode.

X-ray diffraction (XRD) analysis. The X-ray diffraction patterns were conducted on a grazing-incident XRD (Rigaku SmartLab) with Cu K_α at 45 kV. The scanned angle (2θ) ranged from 5° to 60°.

Fourier-transform infrared (FT-IR) analysis. The Fourier-transform infrared (FT-IR) spectra were performed with a Perkin Elmer FTIR-100 spectrometer (USA) with a collected wavenumber range of 500–4000 cm^{-1}.

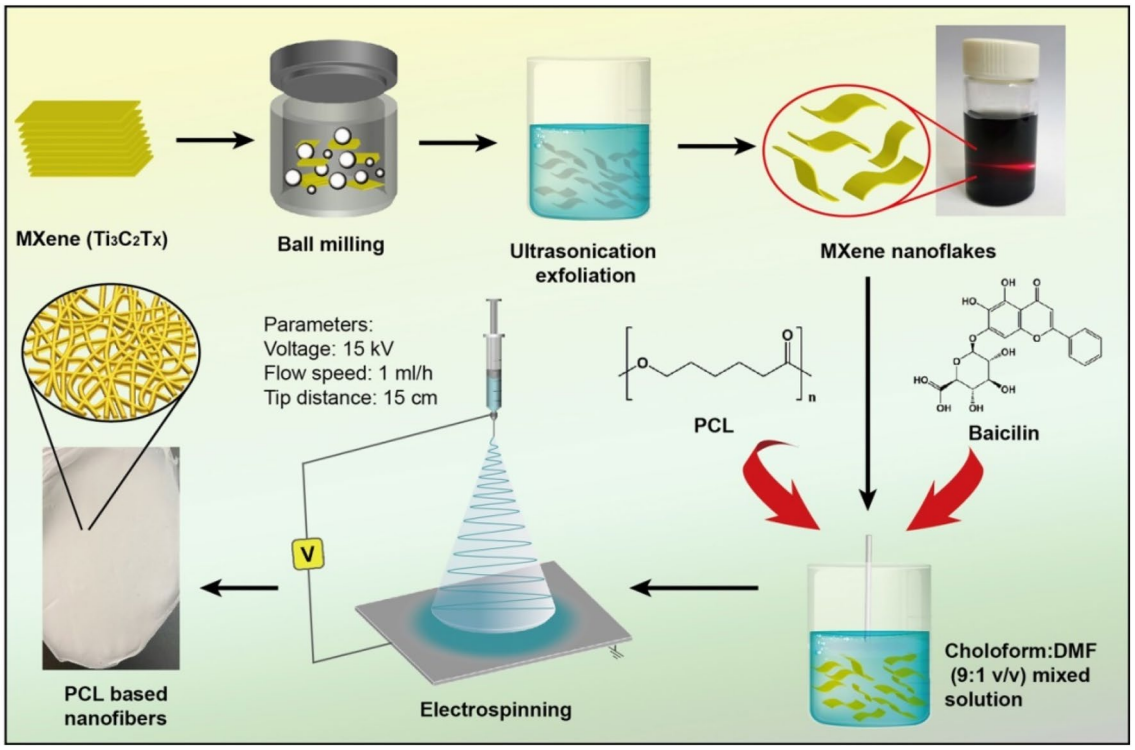

Figure 1. Preparation route of PCL based nanofibers. (Adobe Illustrator CS5, Version 15.0.0, https://www.adobe.com/products/illustrator.html).

Samples	PCL (wt%)	$Ti_3C_2T_X$ (wt%)	Baicalin (wt%)
PCL-0	100	–	–
PCL-1	97	3	–
PCL-2	97	–	3
PCL-3	94	3	3
PCL-4	92	3	5

Table 1. Formulations of PCL based nanofibers.

Thermogravimetric analysis (TGA). The thermal stability was evaluated by a thermogravimetric analyzer (TGA, Netzsch TGA-209F1). The specimens were heated from room temperature to 600 ℃ at a ramping rate of 10 ℃/min.

Water contact angels (WCA). The wettability of the nanofibers was evaluated via the measurement of the water contact angle using a See System E instrument (Advex Instruments, Czech Republic).

Minimum inhibitory concentration (MIC) determination. The standard broth microdilution method was applied to determine the MIC value of baicalin toward *S. aureus* as described in the previous reports[25,26]. Briefly, the *S. aureus* was inoculated and grown in a broth subculture inside a flask. The bacteria were then incubated at 37 °C for 24 h. Then, the bacterial concentration was adjusted to a density of 1.0×10^6 CFU/ml. The baicalin solution, with a concentration ranging from 1 to 1024 mg/ml, was added into the *S. aureus* solution to observe the bacteria's growth. The lowest concentration, at which no visible bacterial growth was observed in the plate, was considered as the MIC.

Antibacterial tests. The antibacterial properties of the PCL based nanofiebers against *S. aureus* were evaluated by a standard "SNV 195920-1992" evaluation model[26]. The evaluation standard of inhibition zone is summarized in Table S1. The Firstly, 100 μL of 10^8 CFU/mL bacteria suspension was spread on an LB agar plate, and then the nanofibrous membrane samples with a diameter of 1.0 cm were placed on the surface of the agar. The bacteria suspension with the PCL-based films were incubated at 37 °C, followed by the digital images of the PCL-based nanofibrous membranes on the agar plate with bacteria were recorded at 24 h, 72 h, and 120 h, respectively. All samples were tested in triplicate.

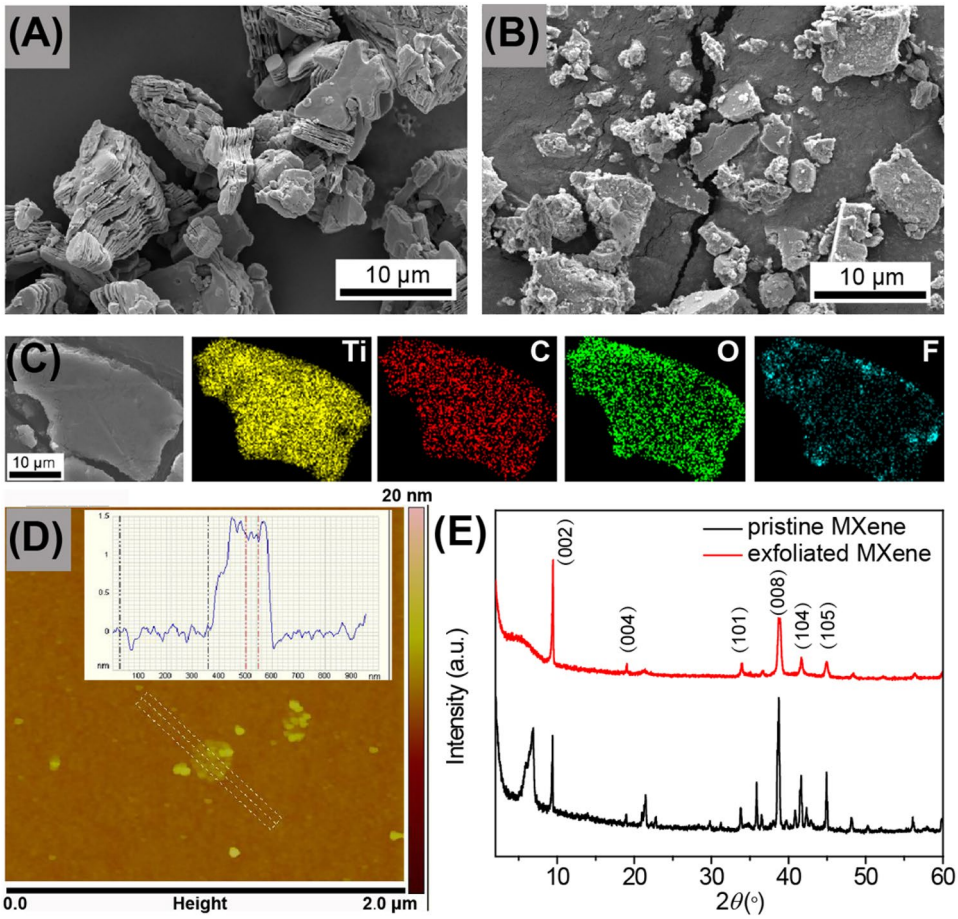

Figure 2. SEM images of **(A)** pristine $Ti_3C_2T_X$, **(B)** exfoliated $Ti_3C_2T_X$ nanoflakes; **(C)** EDX elemental mapping of exfoliated $Ti_3C_2T_X$ nanoflakes, **(D)** AFM image of exfoliated $Ti_3C_2T_X$ nanoflakes, and **(E)** XRD patterns of pristine $Ti_3C_2T_X$ and exfoliated $Ti_3C_2T_X$ nanoflakes.

Cytocompatibility evaluation. The cytotoxicity of the nanofibers on rat skeletal myoblast L6 cells was evaluated using the CCK-8 method with a leaching pattern. The sterilized nanofibers extract solutions (10 mg/mL) were prepared by immersing the dried nanofiber in medium for 12 h at 37 ℃ with ultrasonic extraction. The L6 cells were seeded in a 96-well plate at a density of 5000 cells/well, and pre-cultured for 24 h before replacing the culture medium with the fresh medium and extract solutions to make the final sample concentration of 0.2 mg/mL, 1 mg/mL, and 5 mg/mL. Each sample to be tested (PCL-0, PCL-1, PCL-2, PCL-3, and PCL-4), blank control (culture medium) and positive control (culture medium and cell) were incubated for 48 h and repeated four times. The results were recorded as the absorbance at 450 nm through an ultraviolet spectrophotometer by the following formula:

$$\text{Cell Growth Rate (RGR)} = (\text{Test}_{OD450} - \text{Blank}_{OD450})/(\text{Positive}_{OD450} - \text{Blank}_{OD450}) \times 100\%.$$

Statistical analysis. All experiments were carried out in triplicate. The data was analyzed by the SPSS software (IBM Analytics, USA). Significance of all the statistical tests was predetermined at $P < 0.05$. Results were expressed as mean ± standard deviation (SD).

Results and discussion

Characterization of MXene nanoflakes. In Fig. 2A, the pristine MXene ($Ti_3C_2T_X$) shows a typical organ-like structure with gaps of tens of nanometers wide. The exfoliated $Ti_3C_2T_X$ nanoflakes in Fig. 2B show that the layers are clearly separated from each other. In addition, some small nanoflakes in the range of tens of nanometers are observed due to the grinding. The EDX elemental mapping images in Fig. 2C confirm the presence of Ti, C, and O, which is consistent with the chemical structure of $Ti_3C_2T_X$[20]. The appearance of F on the surface of $Ti_3C_2T_X$ nanoflakes is due to the remaining F element after etching with LiF/HCl[17]. In the AFM image in Fig. 2D, it is observed that the exfoliated $Ti_3C_2T_X$ nanoflake has a thickness of 1.5 nm, which is similar to the reported results[27,28]. The XRD patterns of pristine $Ti_3C_2T_X$ and exfoliated $Ti_3C_2T_X$ nanoflakes are shown in Fig. 2E. It is noted that the characteristic peak at 6.9° in pristine MXene indicates the interlayer spacing of

1.28 nm. In addition, the prominent peaks at 9.4°, 19.1°, 34.0°, 38.7°, 41.7° and 44.9°, which correspond to the diffraction of (002), (004), (101), (008), (104), and (105) planes of $Ti_3C_2T_X$, respectively[29]. As for the exfoliated $Ti_3C_2T_X$ nanoflakes, the characteristic peak shifts from 6.9° to 5.4° due to the exfoliation. In addition, this peak becomes board and weak, which is ascribed to the ball milling and exfoliation reducing the size of the nanoflakes and enlarging the interlayer spacing.

Characterization of PCL nanofibrous membranes. The SEM images of PCL nanofibrous membranes are presented in Fig. 3. It is noted that the nanofibers of PCL-0 with a mean diameter of 269 nm (Fig. 3B) have a smoother surface and non-beaded structures. With the addition of 3 wt% $Ti_3C_2T_X$ nanoflakes, the mean diameter of PCL-1 decreases from 269 to 217 nm as compared with that of PLA-0. In Fig. 3F,H,J, the mean diameters of PCL-2, PCL-3 and PCL-4 are 254 nm, 223 nm, and 210 nm, respectively. It is believed that the presence of conductive $Ti_3C_2T_X$ nanoflakes can increase the charge density of the electrospinning solution due to the polar groups on their surface, thus enhancing the electrostatic force of the applied electric field and reducing the diameter of the nanofibers[30,31]. On the other hand, the introduction of baicalin has little effect on the diameter of the nanofibers. However, the surface of the PCL nanofibers containing baicalin is relatively smoother than that of PCL-1. It is speculated that baiclin is a type of small molecule with many hydroxyl groups that can reduce the viscosity of the electrospinning solution and react with the polar groups of $Ti_3C_2T_X$ nanoflakes to form hydrogen bonds, resulting in the homogeneous dispersion of $Ti_3C_2T_X$ nanoflakes in the PCL matrix.

The typical tensile stress versus strain curves for PCL-based nanofibrous membranes are shown in Fig. S1A, and the corresponding tensile properties are summarized in Fig. S1B. It is noted that the pure PCL membrane shows high ductility (elongation at break of 305%), which is consistent with other published works[32,33]. For PCL-1, the addition of $Ti_3C_2T_X$ nanoflakes results in strong reinforcing effects, increasing the tensile modulus significantly. Although the abundant polar groups on the surface of $Ti_3C_2T_X$ nanoflakes can react with the ester bonds of PCL, the inhibition effects of the rigid nanosheets will be more profound, lowering the plastic flow ability of PCL molecular chains[34]. On the other hand, the PCL-2 shows a clear decrease in both elasticity and strength. In Figure S1B, the elongation at break and tensile strength of PCL-2 are reduced to 178% and 2.58 MPa, respectively. This is because baicalin is a small molecule that has a plasticizing effect on PCL. As for PCL-3, the tensile strength of the samples improved obviously, with a little sacrifice in elongation at break as compared with those of PCL-2. It is speculated that the presence of $Ti_3C_2T_X$ nanoflakes can react with baicalin to form hydrogen bonds to some extent. With the further increase in the baicalin content, the tensile properties of PCL-4 deteriorate progressively, indicating the baicalin exceeds the reaction sites of $Ti_3C_2T_X$ nanoflakes.

The FT-IR spectra of PCL-based nanofibrous membranes are presented in Fig. 4. It is clearly observed that the two characteristic peaks located at 2943 cm^{-1} and 2863 cm^{-1} of PCL-0 correspond to the stretching bands of CH_2 groups. The absorption peak at 1737 cm^{-1} is ascribed to the stretching of the C=O groups, while the peaks at 1294 cm^{-1} and 1184 cm^{-1} belong to the asymmetric and symmetric stretching of the C–O–C groups, respectively. In addition, the characteristic peak at 1243 cm^{-1} denotes the CH_3 vibrations, and 1045 cm^{-1} belongs to C–O stretching and C–H bending[35]. With the incorporation of $Ti_3C_2T_X$ and baicalin, no obvious change is observed in the FT-IR spectra. The ternary composites show a weak and broad peak between 3600 and 3300 cm^{-1}, which is ascribed to the overlapping of the O–H polar groups on the surface of $Ti_3C_2T_X$ and the O–H stretching vibration of baicalin[36]. Furthermore, there is a new characteristic peak at 1609 cm^{-1} that corresponds to the stretching vibration of C=C of phenyl groups from baicalin[37].

The thermal stability of PCL-based nanofibrous membranes was measured by TGA, as shown in Fig. 5. The corresponding data, including the initial weight loss temperature (T_{10}, the temperature at 10% weight loss), the peak weight loss temperature (T_p, the temperature at maximum weight loss rate), and char residues at 600 ℃ are listed in Table 2. It can be observed that PLA-0 shows a distinct weight loss stage from 300 to 420 ℃, which was associated with the pyrolysis of the chemical bond cleavage of PCL chains[38]. The thermal decomposition curve of PCL-1 shifts to a higher temperature, indicating the presence of $Ti_3C_2T_X$ can increase the thermal stability of PCL nanofibers. According to Table 2, the T_{10} and T_p of PCL-1 increases from 361.8 to 365.8 ℃ and from 403.2 to 415.7 ℃, respectively, as compared with that of PLA-0. This is due to the $Ti_3C_2T_X$ nanoflakes serving as a thermal barrier to protect the underlying PCL matrix. In the case of the PCL/$Ti_3C_2T_X$/baicalin ternary nanofibers, the thermal decomposition curves can be roughly divided into two major stages. The initial weight loss stage occurs in the range of 200–370 ℃ due to the thermal decomposition of baicalin. The second stage occurs at around 370–420 ℃, which is related to the pyrolysis of PCL chains. In addition, the T_{10} and T_p of PCL-4 show a decreasing tendency as compared with those of PLA-0, which is ascribed to the low thermal stability of baicalin.

Figure 6 depicts the XRD patterns of PCL-based nanofibrous membranes. As shown in Fig. 6, the PCL-0 has three significant diffraction peaks at $2\theta = 21.3°$, 22.0° and 23.7°, which correspond to the (110), (111), and (200) planes, respectively[39]. In addition, there is also a relatively weak and broad peak at 11.8° in the PCL-0 pattern. The above results indicate that the pristine PCL is in a semi-crystalline state. In the XRD pattern of PCL-1, one additional peak appears at $2\theta = 6.4°$, which is attributed to the (002) plane of $Ti_3C_2T_X$[20]. After the introduction of baicalin, the diffraction angle of PCL at $2\theta = 11.8°$ becomes weaker and shifts to a lower angle, indicating that the physical interaction between PCL and baicilin is altered.

The water contact angles (WCA) of the membrane surfaces were measured to evaluate the hydrophilicity of the PCL-based nanofibrous membranes, as shown in Fig. 7. It is observed that PCL-0 has a hydrophobic surface with a WCA of 127.1° ± 1.3°, which is consistent with previous reports[40,41]. With the addition of $Ti_3C_2T_X$ nanoflakes, the WCA of PCL-1 shows a slight decrease (115.3° ± 5.2°) due to the abundance of –OH groups on the surface of $Ti_3C_2T_X$. When baicilin was introduced into the PCL matrix, the surfaces of the PCL nanofibrous membrances shifted to hydrophobicity. The contact angles for the PCL-2, PCL-3, and PCL-4 are 82.4° ± 5.4°,

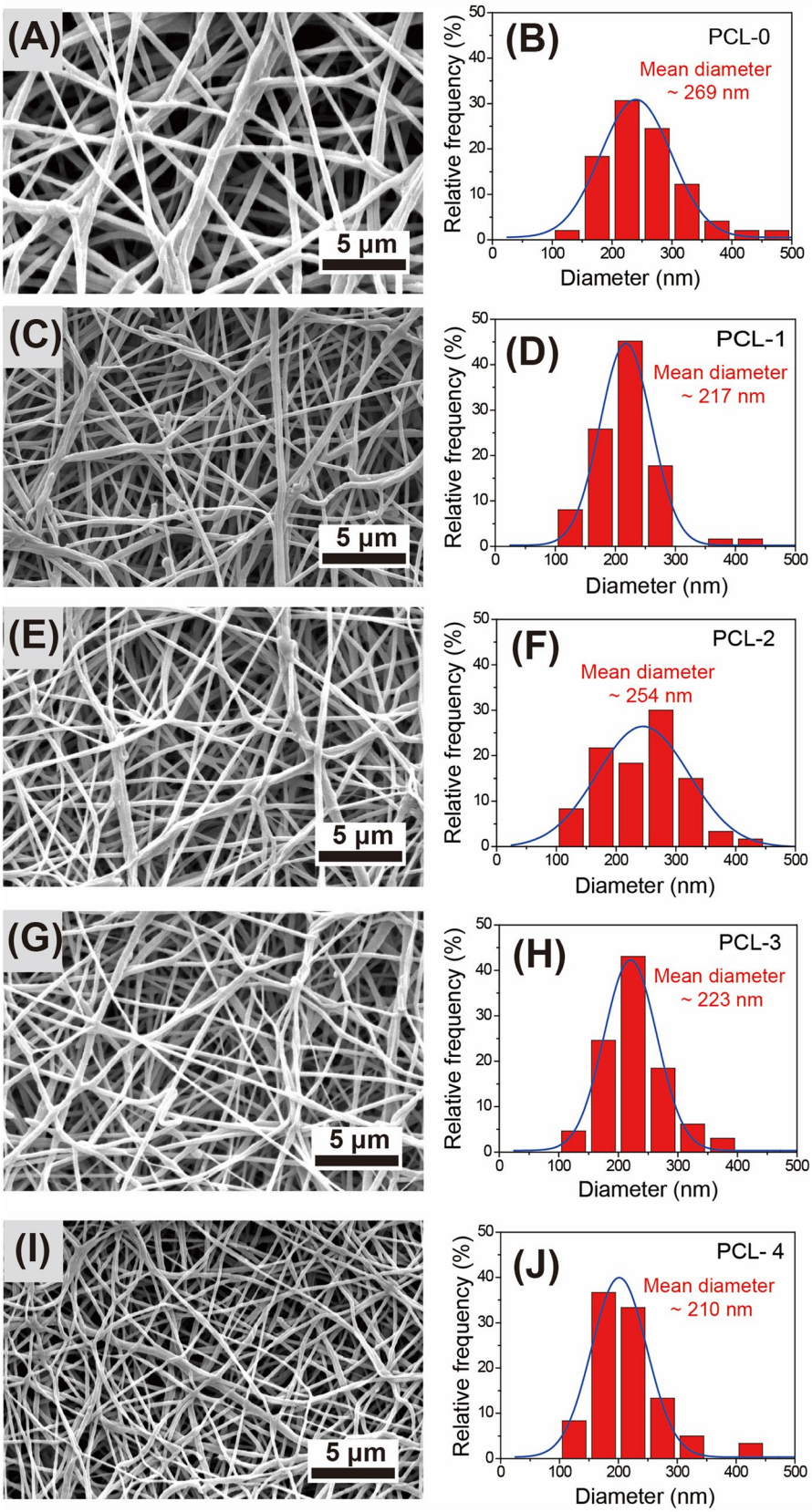

Figure 3 . SEM images of electrospun PCL based nanofibrous membranes and measured fiber diameter distribution: **(A,B)** PCL-0, **(C,D)** PCL-1, **(E,F)** PCL-2, **(G,H)** PCL-3, and **(I,J)** PCL-4.

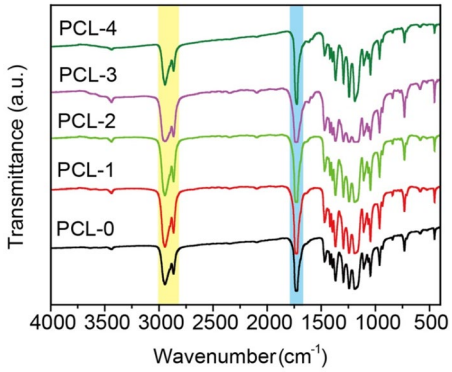

Figure 4. FT-IR spectra of PCL-based nanofibrous membranes.

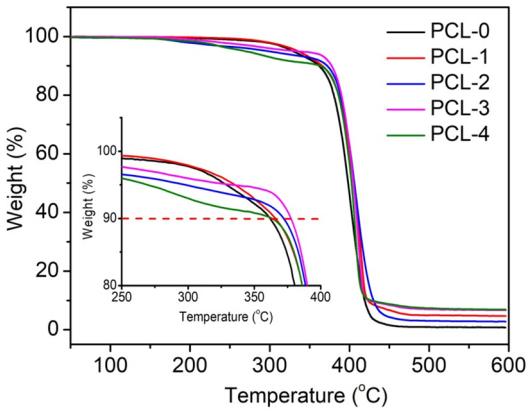

Figure 5. TGA curves of PCL-based nanofibrous membranes.

Samples	T_{10} (℃)	T_p (℃)	Residues at 600 ℃ (wt%)
PCL-0	361.8	403.2	0.73
PCL-1	365.8	415.7	4.71
PCL-2	372.1	408.5	2.79
PCL-3	377.7	412.2	6.65
PCL-4	363.2	407.9	7.38

Table 2. TGA data of PCL-based nanofibrous membranes.

74.4° ± 6.9°, and 65.5° ± 3.2°, respectively. It can be attributed to the fact that baicalin contains a large number of hydrogel groups that increase the hydrophilicity of the electrospun fibers.

Antibacterial activities of PCL nanofibrous membranes. Baicalin is the main antibacterial constituent of PCL-based membranes, which has broad-spectrum antibacterial activity, especially against Gram-positive bacteria like *S. aureus*[42]. In this work, the MIC of baicalin against *S. aureus* was found to be effective at 32 mg/ml, which is similar to the reported literatures[43,44]. All PCL-based nanofibrous membranes were selected for a standard antibacterial test by the preincubation plate pouring method. In Fig. 8, the bacterial colonies appear clustered around the PCL-0 and PCL-1 nanofibrous membranes after 72 h in the detailed pictures, and more remarkable clustered colonies are observed after 120 h. This is due to PCL having no antibacterial ability, which is consistent with previous report[45]. On the other hand, PCL-2, PCL-3, and PCL-4 show obvious bacteriostatic activity at 120 h incubation time (The medium dried completely after 120 h, and further inhibited bacterial growth). It can be ascribed to the presence of baicalin can interrupt the formation of α-heptamer, hindering the cell lysis activity of α-Hemolysin of *S. aureus*[46]. In addition, it is observed that the surrounding areas of PCL-3 and PCL-4 exhibit a light yellow color at 24 h, indicating the addition of $Ti_3C_2T_X$ nanoflakes contributed to the spread of baicalin from the nanofibers. That is because baicalin has poor solubility in aqueous solution[47].

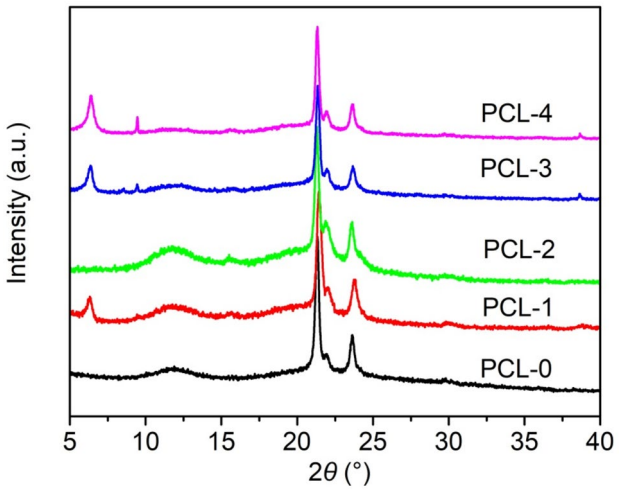

Figure 6. XRD patterns of PCL-based nanofibrous membranes.

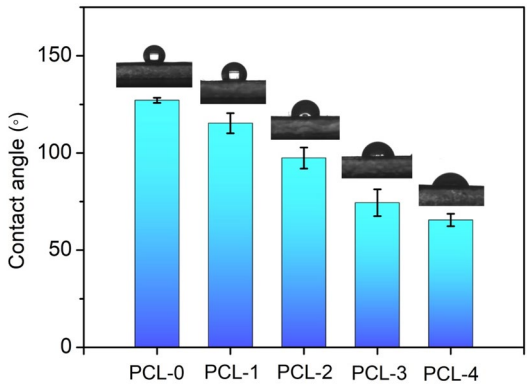

Figure 7. Water contact angle of PCL-based nanofibrous membranes.

Biocompatbility of PCL nanofibrous membranes. The cytotoxicity testing was performed by MTT assays so as to evaluate the biocompatibility of the as-prepared PCL-based nanofiber membrances. It is usually to measure the cell density after the cells have been exposed to the nanofibers' leaching liquor for 48 h to confirm the cytocompatibility of the material. In Fig. 9, it is noted that all groups show no significant cytotoxicity at different concentrations. The cell viability of all test groups modestly declines as the concentration increases. The group with the lowest survival rate remains close to 100% at the highest concentration (5 mg/mL), which suggests that the PCL/$Ti_3C_2T_X$/baicalin ternary nanofibrous membranes can be utilized as safe wound dressings.

Conclusions

In this paper, the electrospun membrances based on PCL/$Ti_3C_2T_X$/baicalin ternary composites were prepared for wound dressing applications. The SEM observation showed that the presence of $Ti_3C_2T_X$ nanoflakes could decrease in the diameter of the nanofibers due to the increase in the charge density of the electrospinning solution. The PCL nanofiber membrances containing 3 wt% $Ti_3C_2T_X$ flakes and 5 wt% baicalin had the smallest mean diameter of 210 nm. The thermal stability of the composite nanofibers was improved due to the barrier effect of $Ti_3C_2T_X$ nanoflakes. The addition of $Ti_3C_2T_X$ and baicalin could enhance the hydrophilicity, contributing to the release of baicalin from the nanofibrous membranes. Furthermore, the addition of baicalin could endow the PCL/$Ti_3C_2T_X$/baicalin ternary nanofibrous membranes with good antibacterial properties. The cytocompatibility test confirmed that all of the PCL-based nanofibrous membranes had good compatibility. The antibacterial PCL/$Ti_3C_2T_X$/baicalin ternary nanofibrous membranes have great potential for wound addressing applications.

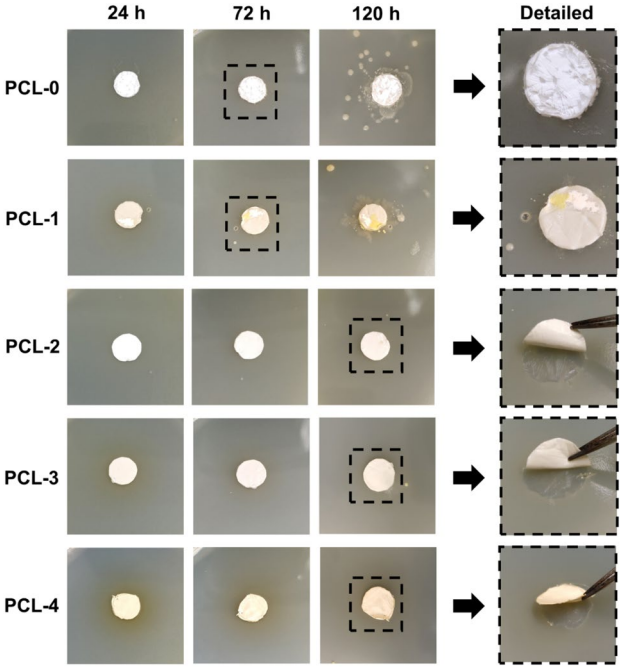

Figure 8. Antibacterial performance of PCL-based membranes against *S. aureus*. (Microsoft Office, PowerPoint 2010, https://www.microsoft.com/zh-hk/microsoft-365/previous-versions/office-2010).

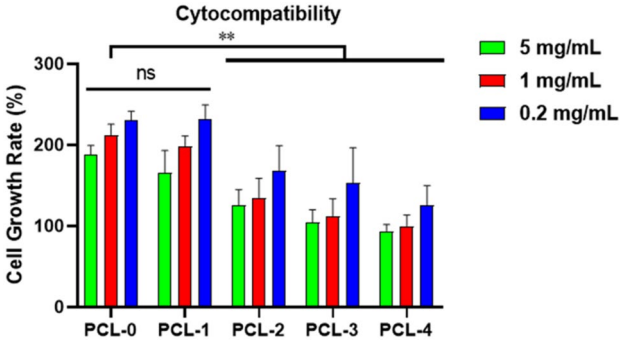

Figure 9. Cytocompatibility of PCL-based membranes. (**$p < 0.01$).

Data availability

The datasets used and/or analyzed during the current study are available from the corresponding author on reasonable request.

Received: 21 December 2021; Accepted: 20 May 2022
Published online: 28 June 2022

References

1. Gravitz, L. Skin. *Nature* **563**, S83 (2018).
2. Jiang, T. C., Wang, Z. Y. & Sun, J. Human bone marrow mesenchymal stem cell-derived exosomes stimulate cutaneous wound healing mediates through TGF-beta/Smad signaling pathway. *Stem Cell Res. Ther.* **11**, 198 (2020).
3. Simoes, D. *et al.* Recent advances on antimicrobial wound dressing: A review. *Eur. J. Pharm. Biopharm.* **127**, 130–141 (2018).
4. Lemraski, E. G. *et al.* Antimicrobial double-layer qound dressing based on chitosan/polyvinyl alcohol/copper: In vitro and in vivo assessment. *Int. J. Nanomed.* **16**, 223–235 (2021).
5. Samadian, H. *et al.* Electrospun cellulose acetate/gelatin nanofibrous wound dressing containing berberine for diabetic foot ulcer healing: In vitro and in vivo studies. *Sci. Rep.* **10**, 8312 (2020).
6. Lanno, G. M. *et al.* Antibacterial porous electrospun fibers as skin scaffolds for wound healing applications. *ACS Omega* **5**, 30011–30022 (2020).
7. Ambekar, R. S. & Kandasubramanian, B. Advancements in nanofibers for wound dressing: A review. *Eur. Polym. J.* **117**, 304–336 (2019).

8. Zahedi, L. *et al.* Development of plasma functionalized polypropylene wound dressing for betaine hydrochloride controlled drug delivery on diabetic wounds. *Sci. Rep.* **11**, 9641 (2021).
9. Hivechi, A. *et al.* Cellulose nanocrystal effect on crystallization kinetics and biological properties of electrospun polycaprolactone. *Mat. Sci. Eng. C-Mater.* **121**, 111855 (2021).
10. Yu, B. R. *et al.* Asymmetric wettable composite wound dressing prepared by electrospinning with bioinspired micropatterning enhances diabetic wound healing. *ACS Appl. Bio. Mater.* **3**, 5383–5394 (2020).
11. Pham, D. D. D. *et al.* Novel lipophosphonoxin-loaded polycaprolactone electrospun nanofiber dressing reduces *Staphylococcus aureus* induced wound infection in mice. *Sci. Rep.* **11**, 17688 (2021).
12. Balcucho, J., Narvaez, D. M. & Castro-Mayorga, J. L. Antimicrobial and biocompatible polycaprolactone and copper oxide nanoparticle wound dressings against methicillin-resistant staphylococcus aureus. *Nanomaterials* **10**, 1692 (2020).
13. Zhu, C. X., Cao, R. F., Zhang, Y. & Chen, R. Metallic ions encapsulated in electrospun nanofiber for antibacterial and angiogenesis function to promote wound repair. *Front. Cell Dev. Biol.* **9**, 660571 (2021).
14. Ghiyasi, Y., Salahi, E. & Esfahani, H. Synergy effect of Urtica dioica and ZnO NPs on microstructure, antibacterial activity and cytotoxicity of electrospun PCL scaffold for wound dressing application. *Mater. Today Commun.* **26**, 102163 (2021).
15. Ekram, B. *et al.* Enhanced mesenchymal stem cells growth on antibacterial microgrooved electrospun zinc chloride/polycaprolactone conduits for peripheral nerve regeneration. *J. Bioact. Compat. Pol.* **36**, 152–168 (2021).
16. Trcin, M. T. *et al.* Poly(epsilon-caprolactone) titanium dioxide and cefuroxime antimicrobial scaffolds for cultivation of human limbal stem cells. *Polymers* **12**, 758 (2020).
17. Wu, W. *et al.* Surface treatment of two dimensional MXene for poly(vinylidene fluoride) nanocomposites with tunable dielectric permittivity. *Compos. Commun.* **23**, 100562 (2021).
18. Zhang, J. B., Fu, Y. & Mo, A. C. Multilayered titanium carbide MXene film for guided bone regeneration. *Int. J. Nanomed.* **14**, 10091–10102 (2019).
19. Zhou, L. *et al.* Conductive antibacterial hemostatic multifunctional scaffolds based on Ti3C2Tx MXene nanosheets for promoting multidrug-resistant bacteria-infected wound healing. *ACS Nano* **15**, 2468–2480 (2021).
20. Liu, C. *et al.* Creating MXene/reduced graphene oxide hybrid towards highly fire safe thermoplastic polyurethane nanocomposites. *Compos. Part B: Eng.* **203**, 108486 (2020).
21. Awasthi, G. P. *et al.* Synthesis, characterizations, and biocompatibility evaluation of polycaprolactone-MXene electrospun fibers. *Colloids Surf. A Physicochem. Eng. Asp.* **586**, 124282 (2020).
22. Xie, J. *et al.* Novel redispersible nanosuspensions stabilized by co-processed nanocrystalline cellulose-sodium carboxymethyl starch for enhancing dissolution and oral bioavailability of baicalin. *Int. J. Nanomed.* **14**, 353–369 (2019).
23. Yang, J. Y., Li, M., Zhang, C. L. & Liu, D. Pharmacological properties of baicalin on liver diseases: A narrative review. *Pharmacol. Rep.* **2019**, 1–10 (2021).
24. Bai, C. F. *et al.* Protective effect of baicalin against severe burn-induced remote acute lung injury in rats. *Mol. Med. Rep.* **17**, 2689–2694 (2018).
25. Matuschek, E., Ahman, J., Webster, C. & Kahlmeter, G. Antimicrobial susceptibility testing of colistin—Evaluation of seven commercial MIC products against standard broth microdilution for *Escherichia coli*, *Klebsiella pneumoniae*, *Pseudomonas aeruginosa*, and *Acinetobacter* spp. *Clin. Microbiol. Infect.* **24**, 865–870 (2018).
26. Wu, W. *et al.* Rhelogical and antibacterial performance of sodium alginate/zinc oxide composite coating for cellulosic paper. *Colloid. Surf. B* **167**, 538–543 (2018).
27. Zhang, J. Z. *et al.* Scalable manufacturing of free-standing, strong Ti3C2Tx MXene films with outstanding conductivity. *Adv. Mater.* **32**, 2001093 (2020).
28. Ayman, I. *et al.* CoFe2O4 nanoparticle-decorated 2D MXene: A novel hybrid material for supercapacitor applications. *Energ. Fuel.* **34**, 7622–7630 (2020).
29. Hu, Z. *et al.* Hierarchical Ti3C2Tx MXene/carbon nanotubes for low overpotential and long-life Li-CO_2 batteries. *ACS Nano* **15**, 8407–8417 (2021).
30. Qiu, Q. H. *et al.* Electrospun nanofibers of polyelectrolyte-surfactant complexes for antibacterial wound dressing application. *Soft Matter* **15**, 10020–10028 (2019).
31. Wu, X. H. *et al.* Hierarchically structured PVP porous fibers derived from the embedding of NaY zeolite synergize the adsorption of benzene. *Compos. Part B Eng.* **179**, 107542 (2019).
32. Castro, A. G. B. *et al.* Development of a PCL-silica nanoparticles composite membrane for guided bone regeneration. *Mat. Sci. Eng. C-Mater.* **85**, 154–161 (2018).
33. Augustine, R., Kalarikkal, N. & Thomas, S. Electrospun PCL membranes incorporated with biosynthesized silver nanoparticles as antibacterial wound dressings. *Appl. Nanosci.* **6**, 337–344 (2016).
34. Augustine, R., Kalarikkal, N. & Thomas, S. Effect of zinc oxide nanoparticles on the in vitro degradation of electrospun polycaprolactone membranes in simulated body fluid. *Int. J. Polym. Mater. Polym. Biomater.* **65**, 28–37 (2016).
35. Wu, W. *et al.* Surface decoration of halloysite nanotubes with POSS for fire-safe thermoplastic polyurethane nanocomposites. *J. Mater. Sci. Technol.* **101**, 107–117 (2022).
36. Escamilla, M. N. *et al.* Rapid determination of baicalin and total baicalein content in *Scutellariae radix* by ATR-IR and NIR spectroscopy. *Talanta* **114**, 304–310 (2013).
37. Jangid, A. K., Jain, P., Medicherla, K., Pooja, D. & Kulhari, H. Solid-state properties, solubility, stability and dissolution behaviour of co-amorphous solid dispersions of baicalin. *CrystEngComm* **22**, 6128–6136 (2020).
38. Liu, Z. N., Zhu, X. Q. & Tang, R. Electrospun scaffold with sustained antibacterial and tissue-matched mechanical properties for potential application as functional mesh. *Int. J. Nanomed.* **15**, 4991–5004 (2020).
39. Jia, Y. T., Huang, G., Dong, F. C., Liu, Q. Q. & Nie, W. L. Preparation and characterization of electrospun poly(epsilon-caprolactone)/poly(vinyl pyrrolidone) nanofiber composites containing silver particles. *Polym. Composite* **37**, 2847–2854 (2016).
40. Li, Y. C. *et al.* Nanofibers support oligodendrocyte precursor cell growth and function as a neuron-free model for myelination study. *Biomacromol* **15**, 319–326 (2014).
41. Song, H. L. *et al.* Hydroxyapatite/NELL-1 nanoparticles electrospun fibers for osteoinduction in none tissue engineering application. *Int. J. Nanomed.* **16**, 4321–4332 (2021).
42. Liu, M. L. *et al.* Nano-silver-decorated microfibrous eggshell membrane: Processing, cytotoxicity assessment and optimization, antibacterial activity and wound healing. *Sci. Rep.* **7**, 1–14 (2017).
43. Li, X. *et al.* The antiviral effect of baicalin on enterovirus 71 in vitro. *Viruses* **7**, 4756–4771 (2015).
44. Liu, I. X., Durham, D. G. & Richards, R. M. E. Baicalin synergy with beta-lactam antibiotics against methicillin-resistant *Staphylococcus aureus* and other beta-lactam-resistant strains of *S-aureus*. *J. Pharm. Pharmacol.* **52**, 361–366 (2000).
45. Felice, B. *et al.* Controlled degradability of PCL-ZnO nanofibrous scaffolds for bone tissue engineering and their antibacterial activity. *Mat. Sci. Eng. C-Mater.* **93**, 724–738 (2018).
46. Qiu, J. Z. *et al.* Baicalin protects mice from *Staphylococcus aureus* pneumonia via Inhibition of the cytolytic activity of alpha-hemolysin. *J. Infect. Dis.* **206**, 292–301 (2012).
47. He, Q., Zheng, M. & Zhao, H. K. Baicalin solubility in aqueous co-solvent mixtures of methanol, ethanol, isopropanol and *n*-propanol revisited: Solvent-solvent and solvent-solute interactions and IKBI preferential solvation analysis. *Phys. Chem. Liq.* **58**, 820–832 (2020).

Author contributions

Investigation, W.Z., N.C., and X.L.; Conceptualization, W.Z., J.J., and Y.L.; Methodology, W.Z., Y.L., X.L., and J.J.; Resources, J.J.; Data curation, H.H., and F.L.; Writing—original draft, W.Z., and N.C.; and Writing—review and editing, J.J., and Y.L.; Supervision, Y.L., and J.J.; All authors have read and agreed to the published version of the manuscript.

Funding

This research was funded by the National Natural Science Foundation of China (grant number 81803339).

Competing interests

The authors declare no competing interests.

Additional information

Supplementary Information The online version contains supplementary material available at https://doi.org/10.1038/s41598-022-13141-0.

Correspondence and requests for materials should be addressed to J.J. or Y.L.

Reprints and permissions information is available at www.nature.com/reprints.

Publisher's note Springer Nature remains neutral with regard to jurisdictional claims in published maps and institutional affiliations.